



A new concept of modal participation factor for numerical instability in the dual BEM for exterior acoustics

J.T. Chen ^{a,*}, K.H. Chen ^a, I.L. Chen ^b, L.W. Liu ^c

^a Department of Harbor and River Engineering, National Taiwan Ocean University, P.O. Box 7-59, Keelung 20224, Taiwan

^b Department of Naval Architecture, National Kaohsiung Institute of Marine Technology, Kaohsiung, Taiwan

^c Department of Civil Engineering, National Taiwan University, Taipei, Taiwan

Received 23 March 2001

Abstract

This paper presents the occurring mechanism why irregular frequencies are imbedded in the exterior acoustics using the dual boundary element method (BEM). The modal participation factor which dominates the numerical instability is derived for continuous and discrete systems. In addition, the irregular (fictitious) frequencies embedded in the singular or hypersingular integral equations are discussed, respectively. It is found that the irregular values depend on the kernels in the integral representation for the solution. A two-dimensional dual BEM program for the exterior acoustics was developed. Numerical experiments are conducted to verify the concept of modal participation factor.

© 2002 Published by Elsevier Science Ltd.

Keywords: Modal participation factor; Fictitious frequency; Exterior acoustics; Dual BEM; Scattering

1. Introduction

Irregular frequencies, or so called fictitious frequencies for exterior acoustics in boundary element method (BEM) or boundary integral equation method (BIEM), have been studied by many researchers (Burton and Miller, 1971; Schenck, 1968) for a long time. For a continuous system, Chen (1998) proved analytically using the dual series model that the positions of fictitious frequencies depend on the kernel in the integral representation for the solution. The types of boundary condition can not change the positions where fictitious frequencies occur once the integral formulation is chosen. Later, Chen and Kuo (2000) applied the theory of circulants to understand the occurring mechanism of irregular frequencies for a discrete system by considering a circular radiator. Numerical examples for nonuniform radiation problems using the dual BEM were provided and irregular frequencies were easily found (Chen et al., 2000). Although the fictitious frequencies can be predicted theoretically (Chen, 1998; Chen and Kuo, 2000), we may not find the positions of numerical instability in the real computation for some cases. How to explain the

* Corresponding author. Tel.: +886-2-24622192-6140; fax: +886-2-246632375.

E-mail addresses: jtchen@mail.ntou.edu.tw, jtchen@ind.ntou.edu.tw (J.T. Chen).

30 reason is not trivial. Very few literature on this topic can be found to the authors' best knowledge. In
31 structural dynamics, the concept of modal participation factor (Chen et al., 1995) is well known for
32 structural engineers. It indicates the weighting how the corresponding mode contributes to the response.
33 This concept can be applied to the excitations of body force, boundary force and boundary support motion.
34 The modal participation factor for both the continuous system (Chen et al., 1996) and discrete system
35 (Chen et al., 1995; Chen et al., 1997) were derived in structural dynamics.

36 In this paper, we will propose the concept of modal participation factor for the numerical instability in
37 the dual BEM for exterior acoustics. A dual BEM program was implemented to examine how the modal
38 participation factor dominates the numerical instability near the fictitious frequency. The nonzero modal
39 participation factor causes the numerical oscillation since the total solution is contaminated by the cor-
40 responding fictitious mode. The positions of fictitious frequencies for the exterior problems using the first
41 equation of the dual BEM (the singular integral equation—*UT* method) or the second equation of the dual
42 BEM (the hypersingular integral equation—*LM* method) will be discussed. Four numerical examples of
43 radiation problems and scattering problems subject to the Dirichlet and Neumann boundary conditions,
44 will be illustrated to show how participation factor contributes numerical instability to the total solution.
45 Numerical results using four approaches, the *UT* method, the *LM* method, the CHIEF method, the Burton
46 and Miller method, will be verified in comparison with the analytical solutions and the DtN results (Harari
47 et al., 1997; Stewart and Hughes, 1997). The modal participation factor for the corresponding modes will be
48 determined to predict the contribution of the numerical instability. To circumvent the problem of numerical
49 instability near the fictitious frequency, the Burton and Miller method (Burton and Miller, 1971) and
50 CHIEF method (Schenck, 1968; Chen et al., 2001) will be employed for comparisons.

51 2. Dual formulation for two-dimensional radiation and scattering problems

52 The governing equation for an exterior acoustic problem is the Helmholtz equation as follows:

$$(\nabla^2 + k^2)u(x_1, x_2) = 0, \quad (x_1, x_2) \in D,$$

54 where u is the acoustic potential, ∇^2 is the Laplacian operator, D is the domain and k is the wave number,
55 which is angular frequency over the speed of sound. The boundary conditions can be either the Neumann
56 or Dirichlet type. Based on the dual formulation, the dual equations for the boundary points are

$$\pi u(x) = \text{CPV} \int_B T(s, x)u(s) dB(s) - \text{RPV} \int_B U(s, x)t(s) dB(s), \quad x \in B, \quad (1)$$

$$\pi t(x) = \text{HPV} \int_B M(s, x)u(s) dB(s) - \text{CPV} \int_B L(s, x)t(s) dB(s), \quad x \in B, \quad (2)$$

59 where CPV, RPV and HPV denote the Cauchy principal value, the Riemann principal value and the
60 Hadamard principal value, $t(s) = \partial u(s)/\partial n_s$, $U(s, x)$ is the fundamental solution,

$$T(s, x) = \frac{\partial U(s, x)}{\partial n_s}, \quad L(s, x) = \frac{\partial U(s, x)}{\partial n_x} \quad \text{and} \quad M(s, x) = \frac{\partial^2 U(s, x)}{\partial n_s \partial n_x},$$

62 B denotes the boundary enclosing D and the U , T , L and M are the four kernels in the dual formulation. By
63 discretizing the boundary into boundary elements, the linear algebraic equations for the dual boundary
64 integral equations can be written as

$$[T_{pq}]\{u_q\} = [U_{pq}]\{t_q\}, \quad (3)$$

$$[M_{pq}]\{u_q\} = [L_{pq}]\{t_q\}, \quad (4)$$

67 where $[U]$, $[T]$, $[L]$ and $[M]$ are the four influence matrices, $\{u_q\}$ and $\{t_q\}$ are the boundary potential and
68 flux, and the subscripts p and q correspond to the labels of the collocation element and integration element,
69 respectively. In order to avoid the problem of fictitious frequency, the Burton and Miller formulation
70 (Burton and Miller, 1971) is employed by combining the dual equations as follows,

$$\left\{ [T_{pq}] + \frac{i}{k} [M_{pq}] \right\} \{u_q\} = \left\{ [U_{pq}] + \frac{i}{k} [L_{pq}] \right\} \{t_q\}, \quad (5)$$

72 where $i^2 = -1$. Also, the CHIEF method Schenck, 1968 by adding the constraints from the interior points
73 is considered for comparisons.

74 3. Modal participation factor for numerical instability—continuous system

75 For simplicity, we propose the concept of modal participation factor by a circular case. By expanding the
76 four kernels in the dual formulation, we have the following degenerate kernels,

$$U(s, x) = \begin{cases} U^i(R, \theta; \rho, \phi) = \sum_{m=-\infty}^{\infty} \frac{\pi}{2} [-iJ_m(kR) + Y_m(kR)] J_m(k\rho) \cos(m(\theta - \phi)), & R > \rho, \\ U^e(R, \theta; \rho, \phi) = \sum_{m=-\infty}^{\infty} \frac{\pi}{2} [-iJ_m(k\rho) + Y_m(k\rho)] J_m(kR) \cos(m(\theta - \phi)), & R < \rho, \end{cases} \quad (6)$$

$$T(s, x) = \begin{cases} T^i(R, \theta; \rho, \phi) = \sum_{m=-\infty}^{\infty} \frac{\pi}{2} [-iJ'_m(kR) + Y'_m(kR)] J_m(k\rho) \cos(m(\theta - \phi)), & R > \rho, \\ T^e(R, \theta; \rho, \phi) = \sum_{m=-\infty}^{\infty} \frac{\pi}{2} [-iJ'_m(k\rho) + Y'_m(k\rho)] J'_m(kR) \cos(m(\theta - \phi)), & R < \rho, \end{cases} \quad (7)$$

$$L(s, x) = \begin{cases} L^i(R, \theta; \rho, \phi) = \sum_{m=-\infty}^{\infty} \frac{\pi}{2} [-iJ_m(kR) + Y_m(kR)] J'_m(k\rho) \cos(m(\theta - \phi)), & R > \rho, \\ L^e(R, \theta; \rho, \phi) = \sum_{m=-\infty}^{\infty} \frac{\pi}{2} [-iJ'_m(k\rho) + Y'_m(k\rho)] J_m(kR) \cos(m(\theta - \phi)), & R < \rho, \end{cases} \quad (8)$$

$$M(s, x) = \begin{cases} M^i(R, \theta; \rho, \phi) = \sum_{m=-\infty}^{\infty} \frac{\pi}{2} [-iJ'_m(kR) + Y'_m(kR)] J'_m(k\rho) \cos(m(\theta - \phi)), & R > \rho, \\ M^e(R, \theta; \rho, \phi) = \sum_{m=-\infty}^{\infty} \frac{\pi}{2} [-iJ'_m(k\rho) + Y'_m(k\rho)] J'_m(kR) \cos(m(\theta - \phi)), & R < \rho, \end{cases} \quad (9)$$

81 where $x = (\rho, \phi)$, $s = (R, \theta)$, J_m and Y_m are the first and second Bessel functions with order m , respectively. It
82 is found that the source and field points are separated in the degenerate kernels of Eqs. (6)–(9). For the
83 boundary densities, u and t , on the circular boundary, we have

$$u(\theta) = a_0 + \sum_{n=1}^{\infty} (a_n \cos n\theta + b_n \sin n\theta), \quad 0 \leq \theta < 2\pi, \quad (10)$$

$$t(\theta) = p_0 + \sum_{n=1}^{\infty} (p_n \cos n\theta + q_n \sin n\theta), \quad 0 \leq \theta < 2\pi, \quad (11)$$

4

J.T. Chen et al. / Mechanics Research Communications xxx (2002) xxx–xxx

86 where a_0, a_n, b_n, p_0, p_n and q_n are the Fourier coefficients for u and t , respectively. For the Dirichlet case, $a_0,$
87 a_n and $b_n(n \geq 1)$ are known, while p_0, p_n and $q_n(n \geq 1)$ need to be determined. By adopting the null-field
88 equation, we have

$$0 = \int_B T^i(s, x)u(s) dB(s) - \int_B U^i(s, x)t(s) dB(s), \quad x \in \bar{D}, \quad (12)$$

90 where \bar{D} is outside the domain of interest D . By substituting the series forms for the kernels of Eqs. (6) and
91 (7) and the boundary densities of Eqs. (10) and (11) into Eq. (12) and using the orthogonal properties of
92 Fourier bases, we have

$$p_0 = -\frac{H_0^{(1)'}(ka)J_0(ka)}{H_0^{(1)}(ka)J_0(ka)}a_0k, \quad (13)$$

$$p_m = -\frac{H_m^{(1)'}(ka)J_m(ka)}{H_m^{(1)}(ka)J_m(ka)}a_mk, \quad m \geq 1, \quad (14)$$

$$q_m = -\frac{H_m^{(1)'}(ka)J_m(ka)}{H_m^{(1)}(ka)J_m(ka)}b_mk, \quad m \geq 1, \quad (15)$$

96 where $H_m^{(1)}$ denotes the first kind Hankel function with order m . By substituting all the boundary unknowns
97 into the field equation, we have

$$\begin{aligned} u(\rho, \phi) &= \sum_{m=0}^{\infty} \left(\frac{H_m^{(1)}(k\rho)}{H_m^{(1)}(ka)} \right) \left(\frac{J_m(ka)}{J_m(ka)} \right) (a_m \cos(m\phi) + b_m \sin(m\phi)) \\ &= \sum_{m=0}^{\infty} \left(\frac{H_m^{(1)}(k\rho)}{H_m^{(1)}(ka)} \right) \left(\frac{J_m(ka)}{J_m(ka)} \right) \sqrt{a_m^2 + b_m^2} \cos(m\phi - \tau), \quad \rho \geq a, \quad 0 \leq \phi < 2\pi, \end{aligned} \quad (16)$$

99 after employing the following identities

$$H_m^{(1)}(ka) = J_m(ka) + iY_m(ka), \quad (17)$$

$$H_m^{(1)'}(ka) = J_m'(ka) + iY_m'(ka), \quad (18)$$

$$Y_m'(ka)J_m(ka) - iY_m(ka)J_m'(ka) = \frac{2}{\pi ka}, \quad (19)$$

103 where τ is the phase lag. By checking all the terms in the derivation, a term of zero divided by zero,
104 $J_m(ka)/J_m(ka)$, can be found in Eqs. (13)–(16) for the case of irregular values such that $J_m(ka) = 0$. This
105 motivates us to define the modal participation factor as $(H_m^{(1)}(k\rho)/H_m^{(1)}(ka))\sqrt{a_m^2 + b_m^2}$ for the term of nu-
106 merical instability, $J_m(ka)/J_m(ka)$, with respect to the corresponding mode $\cos(m\phi - \tau)$. In a similar way, we
107 can derive the modal participation factor, $(H_m^{(1)}(k\rho)/H_m^{(1)}(ka))\sqrt{a_m^2 + b_m^2}$, for the term of numerical insta-
108 bility, $J_m'(ka)/J_m'(ka)$, with respect to the corresponding mode $\cos(m\phi - \tau)$ in the *LM* method (hypersingular
109 equation). Mathematically speaking, the irregular values can not result in any difficulty since the term of
110 zero divided by zero can be directly determined by the L'Hospital's rule. In an easier way, the same two zero
111 terms can be cancelled out straight forward. However, this is not the case in the real calculation since the
112 unknown densities are assumed in a separate way.

113 4. Modal participation factor for numerical instability—discrete system

114 In this section, the modal participation factor for numerical instability resulted from the fictitious fre-
 115 quencies is derived for a discrete system with an arbitrary boundary. By discretizing $2N$ boundary elements
 116 along the boundary and using the SVD technique for U and T matrices in Eq. (3), we have

$$\Phi_U \Sigma_U \Psi_U^\dagger t = \Phi_T \Sigma_T \Psi_T^\dagger u, \quad (20)$$

118 where \dagger denotes the transpose conjugate, Φ_U , Ψ_U , Φ_T and Ψ_T are the unitary matrices, Σ_U and Σ_T are the
 119 diagonal matrices composed by the singular values $\sigma_i^{(U)}$ and $\sigma_i^{(T)}$ of U and T matrices, respectively. By
 120 choosing the $2N$ column vectors in Ψ_U and Ψ_T as bases for t and u , respectively, we have

$$t = \Psi_U \alpha = \sum_{n=-(N-1)}^N \alpha_n \psi_n^{(U)}, \quad (21)$$

122 and

$$u = \Psi_T \beta = \sum_{n=-(N-1)}^N \beta_n \psi_n^{(T)}, \quad (22)$$

124 where α and β are the generalized coordinates. By substituting Eqs. (21) and (22) into Eq. (20), we have

$$\Phi_U \Sigma_U \alpha = \Phi_T \Sigma_T \beta, \quad (23)$$

126 after using the unitary properties for Ψ_U and Ψ_T . When k is a fictitious frequency (k_i), there exists a ϕ_i^\dagger
 127 which satisfies

$$\begin{bmatrix} U^\dagger(k_f) \\ T^\dagger(k_f) \end{bmatrix} \phi_i = 0, \quad (24)$$

129 after using the Fredholm alternative theorem. By taking the transpose conjugate with respect to Eq. (24),
 130 we have

$$\phi_i^\dagger [U(k_f) \quad T(k_f)] = 0. \quad (25)$$

132 Eqs. (24) and (25) are found to be the SVD updating terms and documents (Chen et al., 1999), respectively.
 133 By premultiplying ϕ_i^\dagger with respect to the left hand side and right hand side of the equal sign in Eq. (23), we
 134 have

$$\phi_i^\dagger \Phi_U \Sigma_U \alpha = \phi_i^\dagger \Phi_T \Sigma_T \beta. \quad (26)$$

136 For simplicity of demonstrable purpose, the Dirichlet problem is considered here. Eq. (26) is reduced to

$$\alpha_i = \frac{\sigma_i^{(T)}}{\sigma_i^{(U)}} \beta_i, \quad i \text{ no sum}, \quad (27)$$

138 since ϕ_i is one of the column vectors in Φ_U and Φ_T . By checking the terms in Eq. (27), an undeterminate
 139 term of zero divided by zero, $\sigma_i^{(T)}/\sigma_i^{(U)}$, can be found when k is an irregular value which satisfies
 140 $\sigma_i^{(T)} = \sigma_i^{(U)} = 0$. The modal participation factor can be defined as $(\sigma_i^{(T)}/\sigma_i^{(U)})\beta_i$ for the numerical instability,
 141 with respect to the corresponding mode $\psi_i^{(T)}$ instead of $\phi_i^{(T)}$. In the same way, we can derive the modal
 142 participation factor, $(\sigma_i^{(M)}/\sigma_i^{(L)})\beta_i$, with respect to the corresponding mode $\psi_i^{(M)}$ instead of $\phi_i^{(M)}$ in the LM
 143 method. By considering the special case of a circular radiator, Eq. (20) reduces to

$$\Phi H J \Psi^\dagger t = \Phi H' J \Psi^\dagger u, \quad (28)$$

6

J.T. Chen et al. / Mechanics Research Communications xxx (2002) xxx-xxx

145 where

$$\Phi = \Psi = \frac{1}{\sqrt{2N}} \begin{bmatrix} 1 & (e^{i\frac{2\pi}{2N}})^0 & (e^{-i\frac{2\pi}{2N}})^0 & \dots & (e^{i\frac{2N\pi}{2N}})^0 \\ 1 & (e^{i\frac{2\pi}{2N}})^1 & (e^{-i\frac{2\pi}{2N}})^1 & \dots & (e^{i\frac{2N\pi}{2N}})^1 \\ \vdots & \vdots & \vdots & \vdots & \vdots \\ 1 & (e^{i\frac{2\pi}{2N}})^{2N-2} & (e^{-i\frac{2\pi}{2N}})^{2N-2} & \dots & (e^{i\frac{2N\pi}{2N}})^{2N-2} \\ 1 & (e^{i\frac{2\pi}{2N}})^{2N-1} & (e^{-i\frac{2\pi}{2N}})^{2N-1} & \dots & (e^{i\frac{2N\pi}{2N}})^{2N-1} \end{bmatrix}_{2N \times 2N}, \quad (29)$$

$$H = \begin{bmatrix} H_0^{(1)}(ka) & 0 & 0 & \dots & 0 \\ 0 & H_{-1}^{(1)}(ka) & 0 & \vdots & 0 \\ 0 & 0 & H_1^{(1)}(ka) & \vdots & 0 \\ \vdots & \vdots & 0 & \ddots & 0 \\ 0 & 0 & 0 & 0 & H_N^{(1)}(ka) \end{bmatrix}_{2N \times 2N}, \quad (30)$$

$$J = \begin{bmatrix} J_0(ka) & 0 & 0 & \dots & 0 \\ 0 & J_{-1}(ka) & 0 & \vdots & 0 \\ 0 & 0 & J_1(ka) & \vdots & 0 \\ \vdots & \vdots & 0 & \ddots & 0 \\ 0 & 0 & 0 & 0 & J_N(ka) \end{bmatrix}_{2N \times 2N} \quad (31)$$

149 In a similar way, we can obtain the modal participation factor for each mode using the *UT* and *LM* methods
150 as shown in Tables 1 and 2, respectively.

Table 1
The modal participation factor in the *UT* method (singular equation)

Mode	Participation factor
ψ_0	$\frac{H_0^{(1)'}(ka) J_0(ka)}{H_0^{(1)}(ka) J_0(ka)} \beta_0$
ψ_{-1}	$\frac{H_{-1}^{(1)'}(ka) J_{-1}(ka)}{H_{-1}^{(1)}(ka) J_{-1}(ka)} \beta_{-1}$
ψ_1	$\frac{H_1^{(1)'}(ka) J_1(ka)}{H_1^{(1)}(ka) J_1(ka)} \beta_1$
\vdots	\vdots
$\psi_{-(N-1)}$	$\frac{H_{-(N-1)}^{(1)'}(ka) J_{-(N-1)}(ka)}{H_{-(N-1)}^{(1)}(ka) J_{-(N-1)}(ka)} \beta_{-(N-1)}$
$\psi_{(N-1)}$	$\frac{H_{(N-1)}^{(1)'}(ka) J_{(N-1)}(ka)}{H_{(N-1)}^{(1)}(ka) J_{(N-1)}(ka)} \beta_{(N-1)}$
ψ_N	$\frac{H_N^{(1)'}(ka) J_N(ka)}{H_N^{(1)}(ka) J_N(ka)} \beta_N$

Where $\psi_0, \psi_{-1}, \psi_1, \psi_{-2}, \dots, \psi_{-(N-1)}, \psi_{(N-1)}$ and ψ_N are the $2N$ columns in $\Psi_{2N \times 2N}$ matrices.

Table 2
The modal participation factor in the LM method (hypersingular equation)

Mode	Participation factor
ψ_0	$\frac{H_0^{(1)'}(ka)J_0'(ka)}{H_0^{(1)}(ka)J_0'(ka)}\beta_0$
ψ_{-1}	$\frac{H_{-1}^{(1)'}(ka)J_{-1}'(ka)}{H_{-1}^{(1)}(ka)J_{-1}'(ka)}\beta_{-1}$
ψ_1	$\frac{H_1^{(1)'}(ka)J_1'(ka)}{H_1^{(1)}(ka)J_1'(ka)}\beta_1$
\vdots	\vdots
$\psi_{-(N-1)}$	$\frac{H_{-(N-1)}^{(1)'}(ka)J_{-(N-1)}'(ka)}{H_{-(N-1)}^{(1)}(ka)J_{-(N-1)}'(ka)}\beta_{-(N-1)}$
$\psi_{(N-1)}$	$\frac{H_{(N-1)}^{(1)'}(ka)J_{(N-1)}'(ka)}{H_{(N-1)}^{(1)}(ka)J_{(N-1)}'(ka)}\beta_{(N-1)}$
ψ_N	$\frac{H_N^{(1)'}(ka)J_N'(ka)}{H_N^{(1)}(ka)J_N'(ka)}\beta_N$

151 **5. Numerical examples**

152 **Case 1. A radiation problem (Dirichlet condition)**

153 For the first example, a radiation problem is considered. The governing equation and boundary con-
154 dition are shown in Fig. 1. The normalized analytical solution to this cylinder problem of a radius a is

$$u(\rho, \phi) = \frac{H_4^{(1)}(k\rho)}{H_4^{(1)}(ka)} \cos(4\phi), \quad \rho \geq a, \quad 0 \leq \phi < 2\pi, \quad (32)$$

156 subject to boundary condition $u(a, \phi) = \cos(4\phi)$, where $H_4^{(1)}(k\rho)$ denotes the first-kind Hankel function of
157 the fourth order. Fig. 2 shows the contour plots for the real-part solutions. The positions where the ir-
158 regular values occur can be found in Fig. 3 for the solution $t(a, 0)$ versus k by using either the UT or the LM
159 equation only. It is found that no irregular values can be found between zero to seven since the modal
160 participation factors in the range are all zeros. At the position of $ka \approx 7.6$, the numerical instability appear
161 since the value is the first zero of $J_4(ka)$ with nonzero participation factor for the UT method. Similarly, the

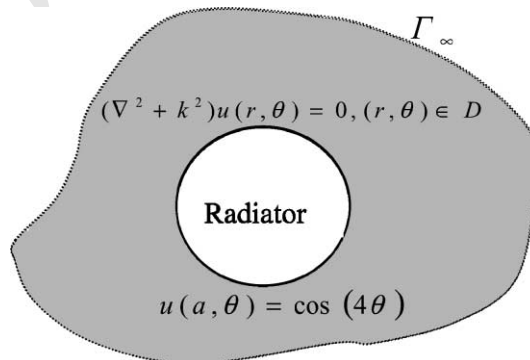


Fig. 1. The uniform radiation problem (Dirichlet condition) for a cylinder.

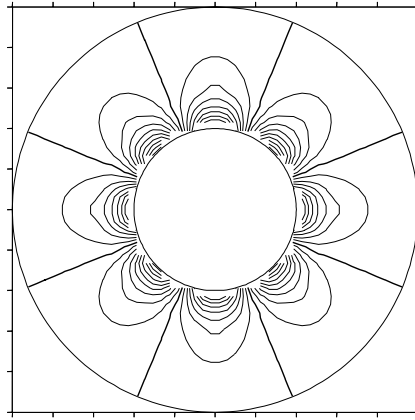


Fig. 2. The contour plot for the real-part solutions.

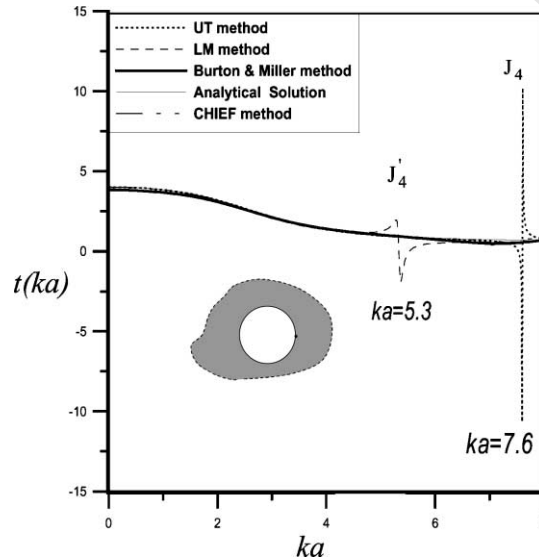


Fig. 3. The positions of irregular values using different methods.

162 irregular value occurs at $ka \approx 5.3$ since the value is the first zero of $J_4'(ka)$ with nonzero participation factor
 163 for the *LM* method. The *UT* and *LM* results agree well as shown in Fig. 2 except at the irregular values. The
 164 performance of the dual BEM in comparison with the analytical solution, CHIEF method, and Burton and
 165 Miller approach is quite good. For engineering applications, CHIEF method may be the first choice for the
 166 practical engineers due to its simplicity. For academic point of view, Burton and Miller approach can avoid
 167 the fictitious frequency in a unified manner without taking any risk of failure.

168 **Case 2.** Nonuniform radiation problem (Neumann condition)

169 In order to clarify how modal participation factor dominates the numerical instability near the fictitious
 170 frequencies, the second example with the nonuniform Neumann boundary condition is designed in Fig. 4.
 171 The analytical solution is

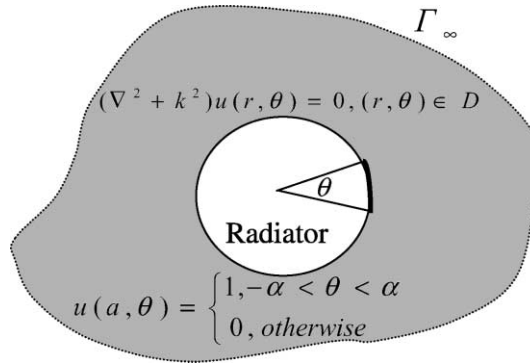


Fig. 4. The nonuniform radiation problem (Dirichlet condition) for a cylinder.

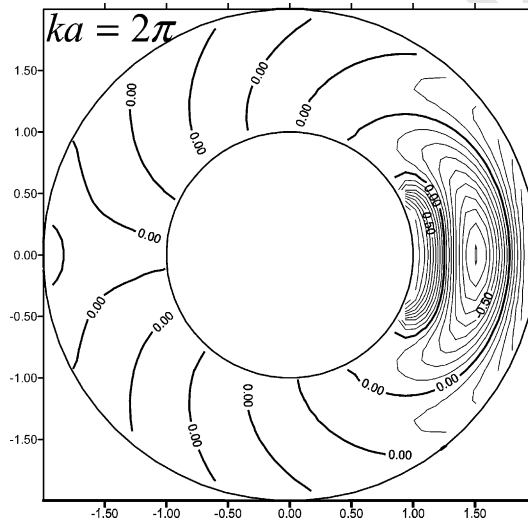


Fig. 5. The contour plot for the real-part solutions.

$$u(\rho, \phi) = \frac{1}{\pi} \frac{-\alpha}{k} \frac{H_0^{(1)}(k\rho)}{H_0^{(1)'}(ka)} + \frac{2}{\pi} \sum_{n=1}^{\infty} \frac{-1}{k} \frac{\sin(n\alpha)}{n} \frac{H_n^{(1)}(k\rho)}{H_n^{(1)'}(ka)} \cos(n\phi), \quad \rho \geq a, \quad 0 \leq \phi < 2\pi. \quad (33)$$

173 Fig. 5 shows the contour plots for the real-part solutions. The irregular frequencies can be clearly found in
 174 Fig. 6 since the modal participation factor is not zero due to nonuniform excitation. Both the J_n and J'_n
 175 zeros are found. It indicates that numerical results agree well with the analytical solution except at the
 176 irregular positions using either *UT* or *LM* method.

177 **Case 3. Scattering problem (Dirichlet condition)**

178 In order to check the validity of the program for scattering problem, example 3 is considered. The in-
 179 cident wave is plane wave and the object is a soft cylinder as shown in Fig. 7. The analytical solution for the
 180 scattering field is

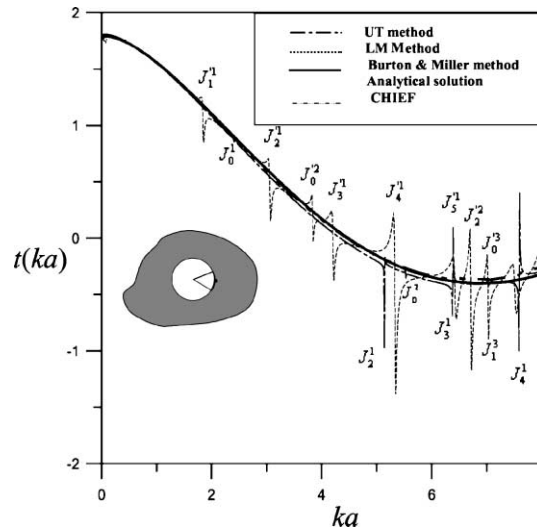


Fig. 6. The positions of irregular values using different methods.

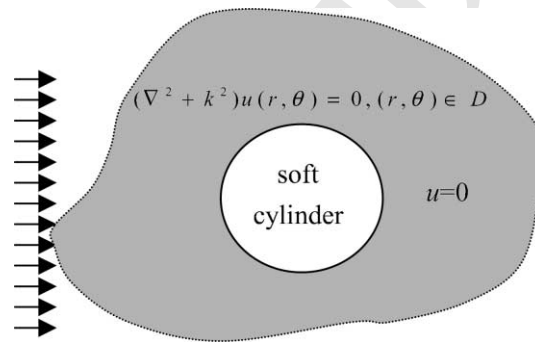


Fig. 7. The scattering problem (Dirichlet condition) for a cylinder.

$$u(\rho, \phi) = -\frac{J_0(ka)}{H_0^{(1)}(ka)} H_0^{(1)}(k\rho) - 2 \sum_{n=1}^{\infty} i^n \frac{J_n(ka)}{H_n^{(1)}(ka)} H_n^{(1)}(k\rho) \cos(n\phi), \quad \rho \geq a, \quad 0 \leq \phi < 2\pi. \quad (34)$$

182 Fig. 8 shows the contour plots for the real-part solutions. The positions where the irregular values occur can
 183 be found in Fig. 9 for the solution $t(a, 0)$ versus k by using either the *UT* or the *LM* equation only. It is
 184 found that irregular values occur at J_n^m , the m th zeros of $J_n(ka)$ for the *UT* formulation, while the *LM*
 185 formulation has the irregular values of J_n^m , the m th zeros of $J_n'(ka) = 0$. In comparing Fig. 9 with Fig. 6, it
 186 indicates that the irregular values are dominated by the chosen method, instead of boundary condition and
 187 problem types. In Fig. 9, it is found that irregular values of J_n^m are more evident than J_n^m after comparing
 188 with the modal participation factors in Tables 1 and 2. The Burton and Miller formulation and the CHIEF
 189 approach are employed to avoid the numerical resonance and the *UT* and *LM* results agree well except at
 190 the irregular wave numbers as shown in Fig. 9. The performance of the dual BEM in comparison with the
 191 analytical solution of Eq. (8) and the DtN results (Harari et al., 1997) is acceptable.

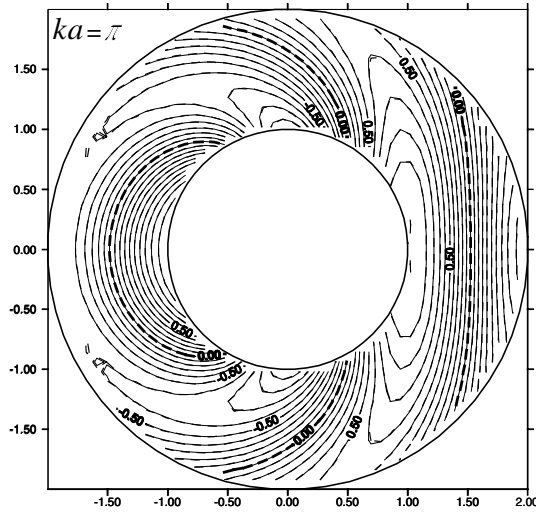


Fig. 8. The contour plot for the real-part solutions (analytical solution: dashed line, numerical result: solid line).

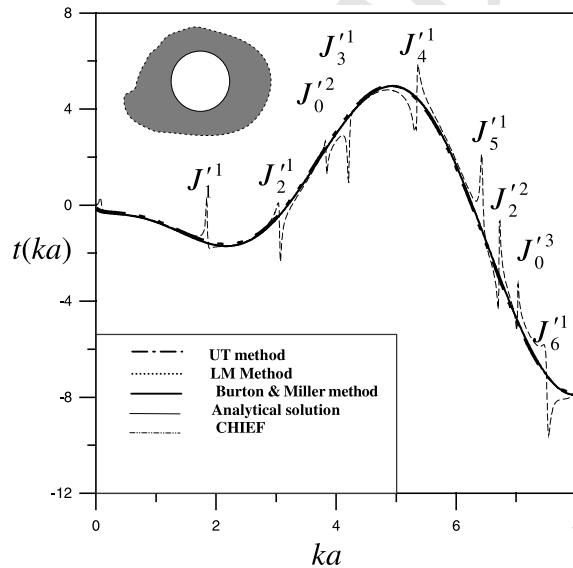


Fig. 9. The positions of irregular values using different methods.

192 **Case 4. Scattering problem (Neumann condition)**

193 In order to clarify how the irregular frequencies depend on the types of boundary conditions, the fourth
 194 example with the Neumann boundary condition is designed. The soft scatter in Example 3 is replaced by a
 195 rigid one in Fig. 10 with the following analytical solution

$$u(\rho, \phi) = -\frac{J'_0(ka)}{H_0^{(1)'}(ka)} H_0^{(1)}(k\rho) - 2 \sum_{n=1}^{\infty} i^n \frac{J'_n(ka)}{H_n^{(1)'}(ka)} H_n^{(1)}(k\rho) \cos(n\phi), \quad \rho \geq a, \quad 0 \leq \phi < 2\pi. \quad (35)$$

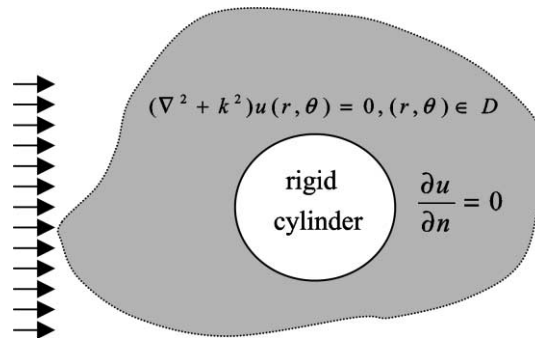


Fig. 10. The scattering problem (Neumann condition) for a cylinder.

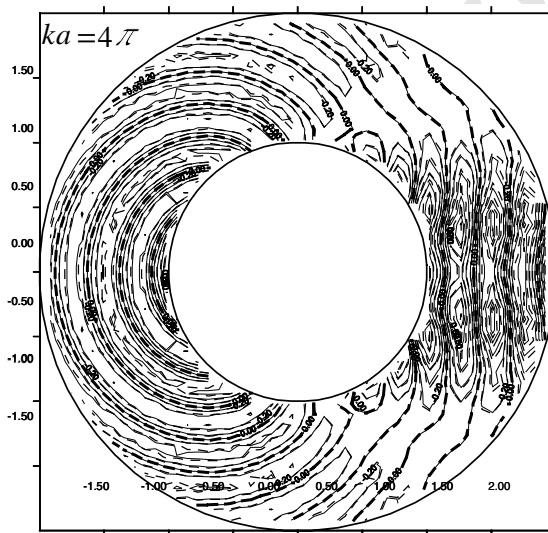


Fig. 11. The contour plot for the real-part solutions (analytical solution: dashed line, numerical results: solid line).

197 Fig. 11 shows the contour plots for the real-part solutions. The positions where the irregular values occur
198 can be found in Fig. 12 for the solution $u(a, 0)$ versus k by using either the *UT* or the *LM* equation only. The
199 performance of the *UT* and *LM* methods in comparison with the analytical solution of Eq. (9), the Burton
200 and Miller solution, the CHIEF solution and the DtN results (Stewart and Hughes, 1997) is quite good
201 except at the positions of irregular values where nonzero participation factors are predicted theoretically.

202 6. Concluding remarks

203 The mechanism why fictitious frequencies occur in the dual BEM has been examined by considering
204 radiation and scattering problems of a cylinder. The concept of modal participation factor for continuous
205 system and discrete system was proposed in a unified way by demonstrating a circular example. It is found
206 that modal participation factor dominates the numerical instability near the irregular frequencies for the

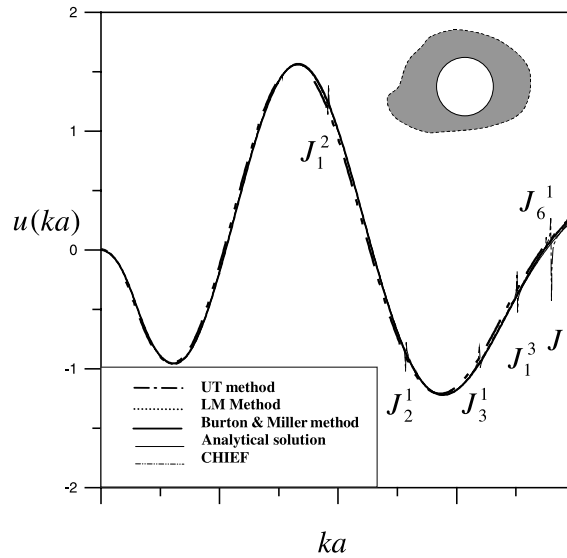


Fig. 12. The positions of irregular values using different methods.

207 corresponding fictitious mode. The irregular values depend on the integral formulation, either the *UT*
 208 (singular) or the *LM* (hypersingular) equation, instead of the types of boundary condition (Dirichlet or
 209 Neumann). Also, the radiation and scattering problems have the same fictitious frequencies once the
 210 method is chosen. The concept of zero modal participation factor can explain why the numerical instability
 211 near the predicted fictitious frequencies may not appear in the numerical experiments and was demon-
 212 strated in the numerical results. All the examples show that the singular (*UT*) equation results in fictitious
 213 frequencies at the zeros of $J_n(ka) = 0$, which are associated with the interior eigenfrequencies of essential
 214 homogeneous boundary conditions, while the hypersingular (*LM*) equation produces fictitious frequencies
 215 at the zeros of $J'_n(ka) = 0$, which are associated with the interior eigenfrequencies of natural homogeneous
 216 boundary conditions. The numerical results using the dual BEM program agree very well with the ana-
 217 lytical solutions and the DtN results except at and near the irregular values. For comparisons, the Burton
 218 and Miller approach and the CHIEF method were successfully employed to deal with the problem of
 219 numerical instability near the fictitious frequency.

220 Acknowledgements

221 Financial support from the National Science Council, under grant no. NSC-91-2211-E-019-009, for
 222 National Taiwan Ocean University is gratefully acknowledged.

223 References

- 224 Burton, A.J., Miller, G.F., 1971. Proc. R. Soc. London Ser. A 323, 201.
 225 Chen, J.T., 1998. Mech. Res. Commun. 25, 529.
 226 Chen, J.T., Chen, C.T., Chen, K.H., Chen, I.L., 2000. Mech. Res. Commun. 27, 685.
 227 Chen, I.L., Chen, J.T., Liang, M.T., 2001. J. Sound Vib. 248 (5), 809.
 228 Chen, J.T., Chyuan, S.W., You, D.W., Wong, F.C., 1997. Finite Elements Anal. Des. 26, 129.

- 229 Chen, J.T., Hong, H.-K., Yeh, C.S., 1995. Commun. Numer. Meth. Engng. 11, 479.
230 Chen, J.T., Kuo, S.R., Cheng, Y.C., 1999. IUTAM/IACM/IABEM Symposium, Cracow.
231 Chen, J.T., Hong, H.-K., Yeh, C.S., Chyuan, S.W., 1996. Earthquake Eng. Struct. Dynam. 25, 909.
232 Chen, J.T., Kuo, S.R., 2000. Mech. Res. Comm. 27, 49.
233 Harari, I., Barbone, P.E., Montgomery, J.M., 1997. Int. J. Numer. Meth. Eng. 40, 2791.
234 Schenck, H.A., 1968. J. Acoust. Soc. Amer. 44 (1), 41.
235 Stewart, J.R., Hughes, T.J.R., 1997. Computer Methods Appl. Mech. Engng. 146, 65.

UNCORRECTED PROOF